Archives of Mechanics • Archiwum Mechaniki Stosowanej • 30, 4–5, pp. 393–409, Warszawa 1978

Characteristics of turbulence in a three-dimensional turbulent boundary layer

R. DECHOV and K. O. FELSCH (KARLSRUHE)

EXTENSIVE experiments were carried out in a three-dimensional incompressible turbulent boundary layer growing in front of a cylinder standing on a flat wall in a wind tunnel. Beginning with the quasi two-dimensional boundary layer far in front of the development of the boundary layer profiles were investigated along a streamline of the free stream up to the region behind the "three-dimensional" separation. At 14 different stations, profiles were measured of the mean velocity vector, the 6 components of the turbulent stress tensor, the static pressure and in addition the wall shear stress vector. The turbulence measurements were carried out with a single hot wire probe and with a rotatable X-probe, whose axis could be aligned with the direction of the local mean velocity. From this data the direction of the velocity gradient and of the turbulent shear stress were evaluated. The applicability of different shear stress models is checked and discussed.

Przeprowadzono szereg doświadczeń w trójwymiarowej nieściśliwej warstwie przyściennej powstałej na czole walca umieszczonego na płaskiej ściance w tunelu aerodynamicznym. Poczynając od quasi-dwuwymiarowej warstwy przyściennej oddalonej od czoła występowania profilów warstwy przyściennej, zbadano profile wzdłuż linii prądu przepływu swobodnego aż do obszaru za trójwymiarowym oderwaniem się strug. W 14 różnych położeniach mierzono: profile wektora uśrednionej prędkości, 6 składowych turbulentnego tensora naprężenia, ciśnienie statyczne oraz dodatkowo tensor naprężeń ścinających na ściance. Pomiary turbulencji przeprowadzono za pomocą pojedynczego czujnika z gorącym drucikiem oraz obrotowego czujnika X, którego oś można ustawić w kierunku lokalnej prędkości średniej. Z danych tych wyliczono kierunek gradientu prędkości i turbulentne naprężenie ścinające. Sprawdzono i przedyskutowano stosowalność różnych modeli naprężeń ścinających.

Проведен ряд экспериментов в трехмерном несжимаемом пограничном слое, возникающем на торце цилиндра помещенного на плоской стенке в аэродинамической трубе. Начиная с квазидвумерного пограничного слоя, находящегося на расстоянии от фронта выступания профилей пограничного слоя, исследованы профили вдоль линий тока свободного течения вплоть до области за трехмерным отрывом струй. В 14 разных положениях измерялись: профили вектора усредненной скорости, 6 составляющих турбулентного тензора напряжений, статическое давление и дополнительно тензор напряжений сдвига на стенке. Измерения турбулентности проведены при помощи единичного датчика с горячей проволокой и вращательного датчика X, ось которого можно установить в направлении локальной средней скорости. Из этих данных вычислены направление градиента скорости и турбулентное напряжение сдвига. Проверена и обсуждена применяемость разных моделей напряжений сдвига.

Nomenclature

c wall-parallel component of the mean velocity,

c_1, c_2, c_3 fluctuating velocity components (see Fig. 4),

c_p pressure coefficient,

l mixing length,

s magnitude of the mean velocity in the boundary layer (see Fig. 4),

s_1, s_2, s_3 fluctuating velocity components (see Fig. 4),

u_{Bez} reference velocity ($u_{\delta 1} = 22.7$ m/s; $u_{\tau 1} = 0.879$ m/s),
u_σ mean velocity at the edge of the boundary laver,
u_τ friction velocity,
u, v, w components of the mean velocity (see Fig. 4),
x, y, z boundary layer coordinates,
α flow angle at the edge of the boundary layer relative to the tunnel axis (see Fig. 4),
β flow angle inside the boundary layer relative to the wall (pitch, upwash) (see Fig. 4),
ν_e eddy viscosity,
γ flow angle inside the boundary layer relative to the x-y-plane (yaw) (see Fig. 4),
γ_G angle of the velocity gradient vector relative to the x-y-plane,
γ_τ angle of the wall-parallel component of the shear stress vector relative to the x-y-plane,
ϱ density,
τ magnitude of shear stress vector,
τ_w wall shear stress.

1. Introduction

FOR THE DEVELOPMENT of better calculation methods for three-dimensional turbulent boundary layers more data are urgently needed, in particular data concerning the behaviour of the turbulence properties. Recent meetings where discussions were held on this subject, (e.g. Euromech 60 in Trondheim 1975) confirm this necessity. The purpose of this paper is to contribute new data to this problem.

V. d. BERG *et al.* [1] and FLSENAAR *et al.* [2] have made complete measurements in a three-dimensional layer of the infinite swept wing type; in the present case data of a more general type are to be presented, that is, data obtained in a three-dimensional boundary layer in front of an obstruction mounted upon a flat plate. As in the case of EAST *et al.* [3] (who only made measurements of the mean velocity) the obstruction is a cylindrical body, and the boundary layer on the flat plate in front of the body is to be investigated.

2. Description of the working section

The measurements were carried out in the boundary layer wind tunnel of the Institut für Strömungslehre und Strömungsmaschinen of the University of Karlsruhe. Figure 1 shows the sketch of the working section which is a rectangular duct of a 1500 mm × 300 mm cross section and a 3000 mm length. The cylinder diameter is 320 mm with a streamlined afterbody which prevents separation. The cylindrical body extends from the floor to the roof, the working area being near to the floor. The boundary layer probes are mounted in a probe-holder which is movable normal to the walls and can be rotated around the axis normal to the walls by a traversing mechanism. The probe-holder fits through slots in the upper wall of the working section and can be shifted together with the traversing gear along the slots whose direction is parallel to the tunnel axis. In addition, a part of the roof plate

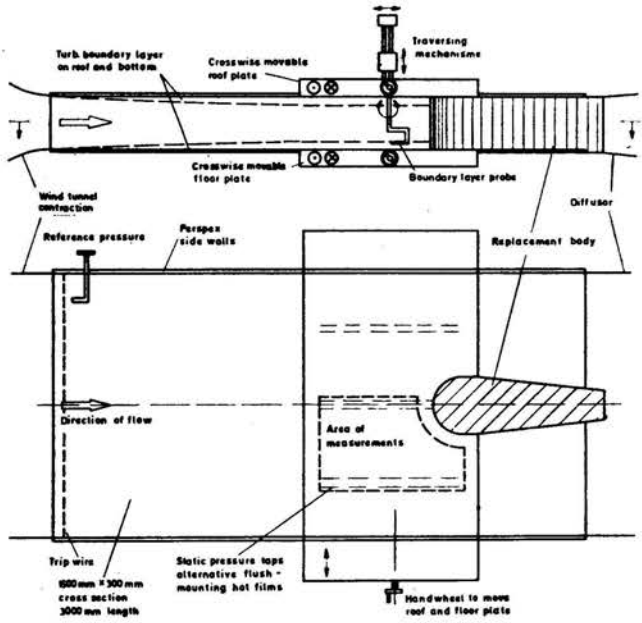

FIG. 1. Working section of boundary layer wind tunnel.

is movable spanwise together with the probe. The floor plate is designed in a similar manner with pressure taps and the possibility of inserting flush-mounted hot films. This design of the working section allows every point of the working area to be reached by the probes.

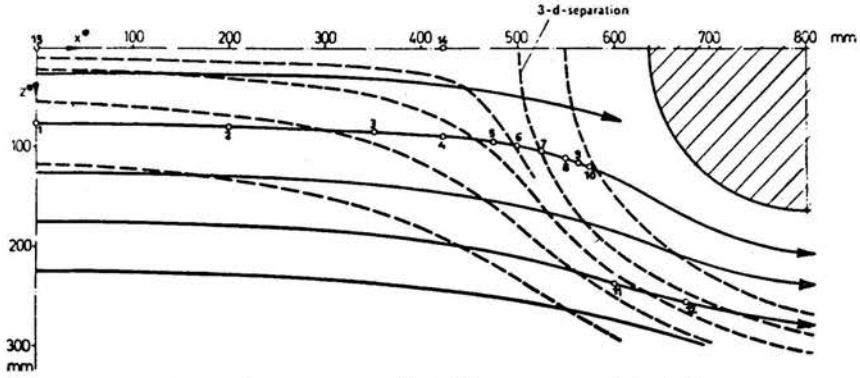

FIG. 2. Streamline patterns and positions of measuring stations;
——— streamlines at $y = \delta$, — — — wall streamlines (from oil flow pattern), positions of measuring stations.

Figure 2 shows some streamlines in the working section; the wall streamlines were determined from an oil flow pattern, whereas the lines in the free stream are drawn from direction measurements with a Conrad-tube. The quasi two-dimensionality at the start of the working area and the strong three-dimensionality in the region of separation can easily

be seen. In this region there exist large gradients of the mean velocity in all directions and the vector of the mean velocity carries a component normal to the wall which is not negligible. These two facts are important; the first for the critical examination of the results of this work, the second for the applicability of the different measurement techniques.

3. Measuring program

In addition to the direction of the streamlines in the free stream the magnitude of the velocity and the static pressure were also measured, as was the static pressure at the wall. The isobars in the free stream and at the wall are shown in Fig. 3 where one can see the large differences near the cylinder.

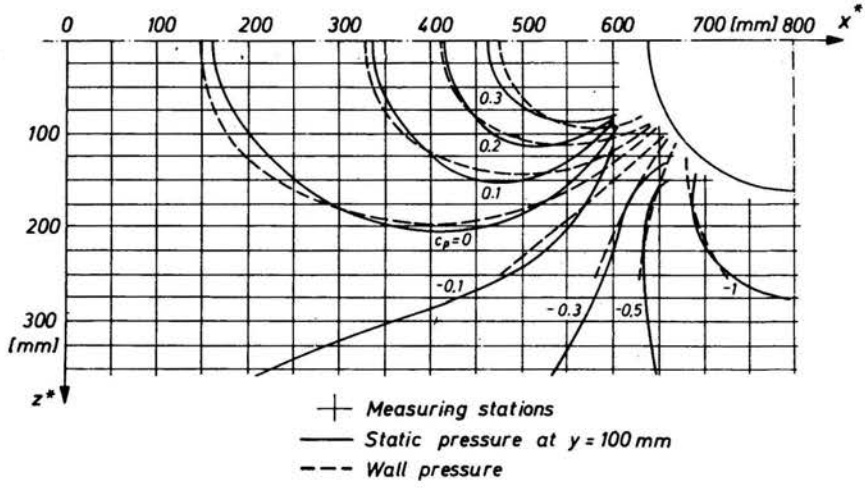

FIG. 3. Static pressure at the wall and in the free stream; ——— pressure at $y = 100$ mm, — — — wall pressure.

One streamline in the free stream was chosen (see Fig. 2) along which the boundary layer profiles were investigated at 10 separate stations (Nos 1—10). In addition, 2 stations (Nos 11 and 12) on a streamline further removed from the cylinder and 2 stations (Nos 13 and 14) on the median plane were chosen. At these 14 stations the following variables were measured:

I) the vector of the mean velocity,
II) the 6 components of the Reynolds stress tensor,
III) the static pressure and
IV) the value and direction of the wall shear stress.

For presentation purposes a streamline coordinate system is used where the x-axis is aligned with the direction of the mean velocity at the edge of the boundary layer and projected onto the wall at every station. Figure 4 show the symbols used for the mean velocity and the fluctuating velocity components.

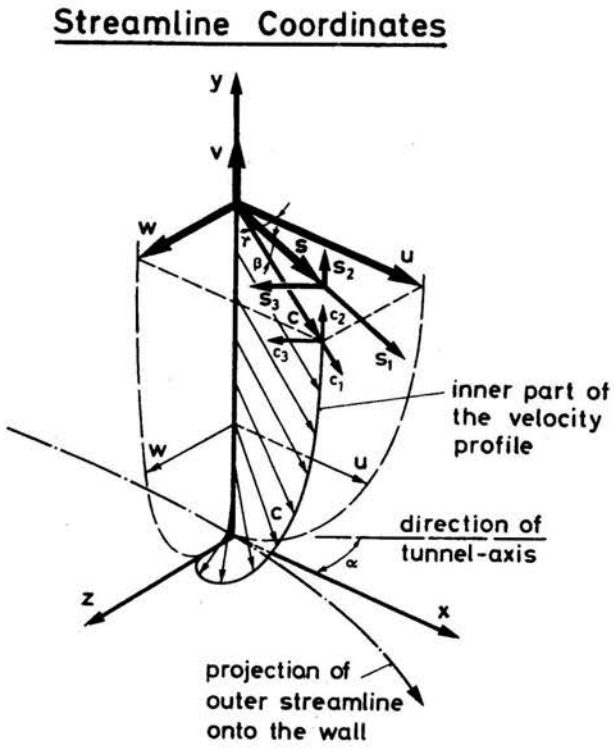

FIG. 4. Streamline coordinates and symbols used for the mean velocity and the fluctuating velocity components.

4. Experimental methods

In the free stream area the value of the mean velocity u was measured with a Pitot-tube and a static pressure probe after evaluation of its direction with a Conrad-tube. Inside the boundary layer the value of the mean velocity vector s, the yaw angle γ and the turbulence intensity $\sqrt{s_1^2}$ were measured with a boundary layer type single hot-wire sensor with gold plated ends. The pitch angle β and the remaining 5 components of the stress tensor were measured with an X-probe. The design of the probe holder allowed for yawing around the y-axis, pitching relative to the wall and turning around the probe axis without the probe tip leaving the measurement point. It was thus possible to align the probe axis with the local direction of the mean velocity s. Figure 5 shows the X-probe in the test section. Due to this alignment the two wires of the X-probe are equally sensitive to the fluctuating component in the direction of the local mean velocity and to the component normal to the mean velocity which lies in the plane formed by the wire and the mean velocity. By turning the X-probe around its axis in steps of 45 degrees combined with suitable processing of the signals the 6 components of the Reynolds stress tensor can be evaluated. After calibration and linearization of the wire signals this kind of evaluation needs neither further assumptions nor corrections and it is the consistent application of the X-probe methods described by

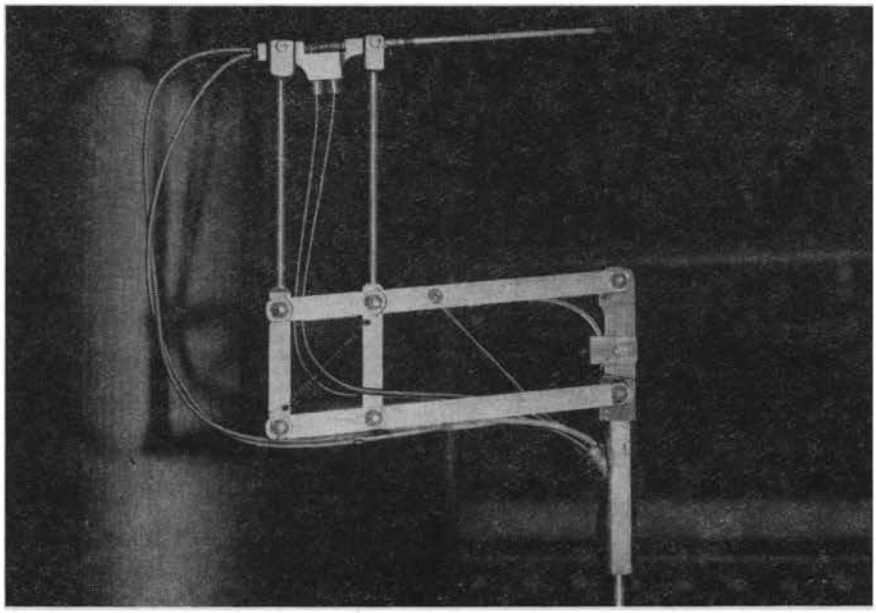

FIG. 5. *X*-probe and probe holder in the test section.

HINZE [4] and BRADSHAW *et al.* [5] It seems to be comparatively accurate. This of course is only valid if the influence of temperature, dust, electronic drift, mal-positioning of the probe, imperfections in the manufacturing of the probe and, last but not least, the influence of the non-uniform flow field as well as the turbulence intensity are properly taken into consideration.

The static pressure inside the boundary layer was evaluated with the usual disc-probe; pressure taps were used for the wall pressure. The value of the wall shear stress was measured with a Preston-tube. The direction of the wall streamlines was evaluated in 3 different ways:

I) from the oil flow pattern,

II) by extrapolating the direction of the mean velocity at a wall distance $y = 0.2$ mm and

III) with a turnable flush-mounted hot-film probe.

5. Presentation of the measurements

In this section the most important results of the measurements will be shown. For the whole data set see DECHOV [6].

In the first part the governing flow parameters are shown along the streamline described in Sect. 3 and marked in Fig. 2. This will explain the nature of the flow at the edge of the boundary layer and will be helpful for the later understanding of the boundary layer data.

5.1. Flow parameters along the streamline

Figure 6 shows the flow parameters plotted against the x-coordinate, which follows the projection of the streamline on the wall. Along this streamline the development of the boundary layer was investigated at Stations 1 to 10 (see Fig. 2). The measurements at

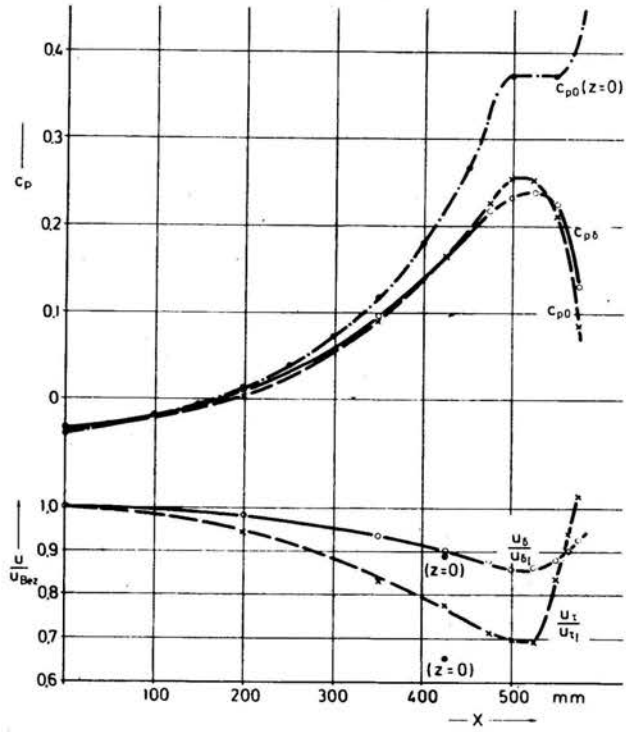

FIG. 6. Static pressure coefficient, free stream velocity and friction velocity along the measured streamline and on centerline.

Stations 11 to 14 were made for the purpose of comparison. In the upper part of Fig. 6 the pressure coefficient c_p is drawn; $c_{p\delta}$ is the pressure at the edge of the boundary layer, c_{p0} its value at the wall. The wall pressure on the centerline c_{p0} ($z = 0$) is included for comparison.

The lower part shows the mean velocity u_δ and the friction velocity u_τ, both made dimensionless with their values at Station 1. In this part only one value on the centerline ($z = 0$) is included for u_τ and u_δ.

The figure shows a small deceleration of the velocity up to the line of three-dimensional separation ($x \approx 520$ mm) and an acceleration after this line. In the region of acceleration the friction velocity grows much faster than the velocity at the edge. This follows the development of the static pressure, which drops more sharply at the wall than at the edge. The velocity profiles will show later a strong acceleration near the wall in this region. All these facts are well matched.

The directions relative to the tunnel of the free streamline, that is the angle α, and of the near-wall streamlines, that is the sum of α and the yaw angle γ near or at the wall, are shown in Fig. 7. Again there is a strong change at the wall in the region near the so-call-

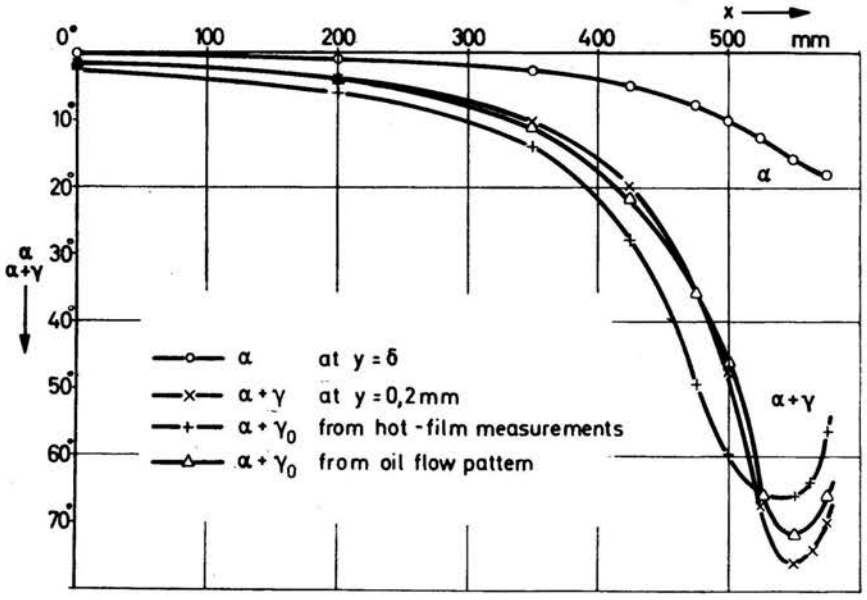

FIG. 7. Direction of streamlines.

ed three-dimensional separation. The different measurements show different directions in this region. This can be interpreted by the different measuring methods and by the nature of the flow.

5.2. Boundary layer profiles

Figures 8 to 15 indicate the results of the measurements taken at the 10 stations on the streamline. In each of these figures the parameters are non-dimensionalized and plotted against the wall distance y in mm. The components u and w of the mean velocity are plotted in Figs 8 and 9 non-dimensionalized by u_δ. The turbulence intensities were measured in the components s_1, s_2 and s_3 relative to the mean velocity s. They will be shown here after conversion to the components c_1, c_2 and c_3 relative to the mean velocity component c parallel to the wall (see Fig. 4). Figures 11 to 13 show the *rms*-values of the intensities c_1, c_2 and c_3 non-dimensionalized by the friction velocity u_τ. In Figs. 13 to 15 the shear stress components $\overline{c_1 c_2}$, $\overline{c_2 c_3}$ and $\overline{c_1 c_3}$ are plotted, this time non-dimensionalized with u_τ^2. It may be noted that the third shear stress component $\overline{c_1 c_3}$ (which is usually neglected in the 3-D boundary layer theory) can have quite significant values.

The mean velocity profile at Station 1 is a quasi two-dimensional one; the profiles of the fluctuating components and of the shear stress ($\overline{c_1 c_2}$) are in good agreement with the flat plate boundary layer data of KLEBANOFF [7]. Further downstream the increasing influence

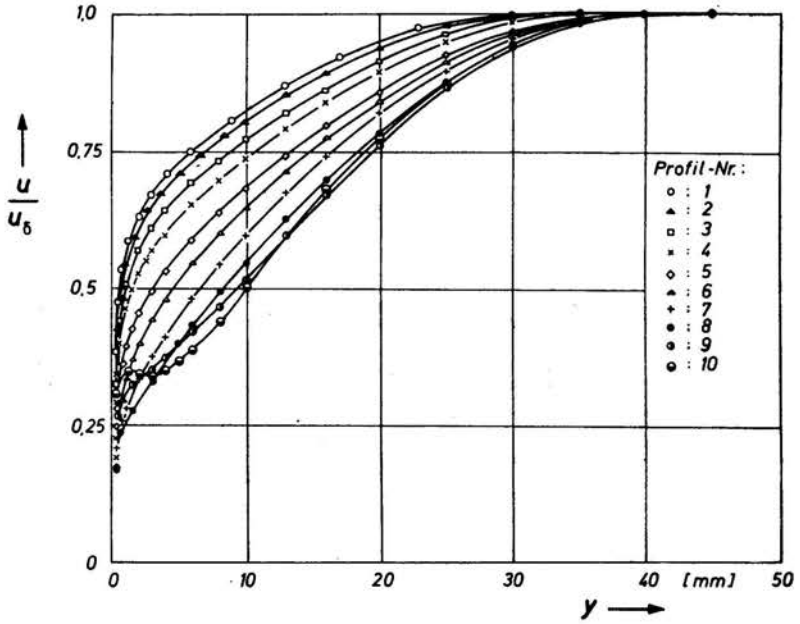

FIG. 8. Component u of the mean velocity.

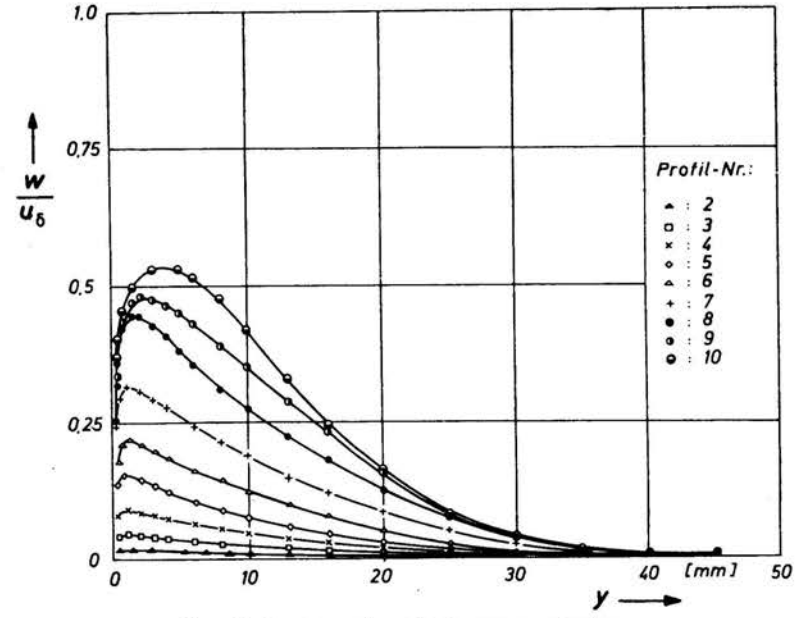

FIG. 9. Component w of the mean velocity.

of three-dimensionality can be seen clearly. The data at Stations 1 to 7 correspond well to the measurements of v.d. BERG *et al.* [1] and ELSENAAR *et al.* [2], whereas at Stations 8 to 10 the shape of the profiles deviates widely from that observed normally in three-di-

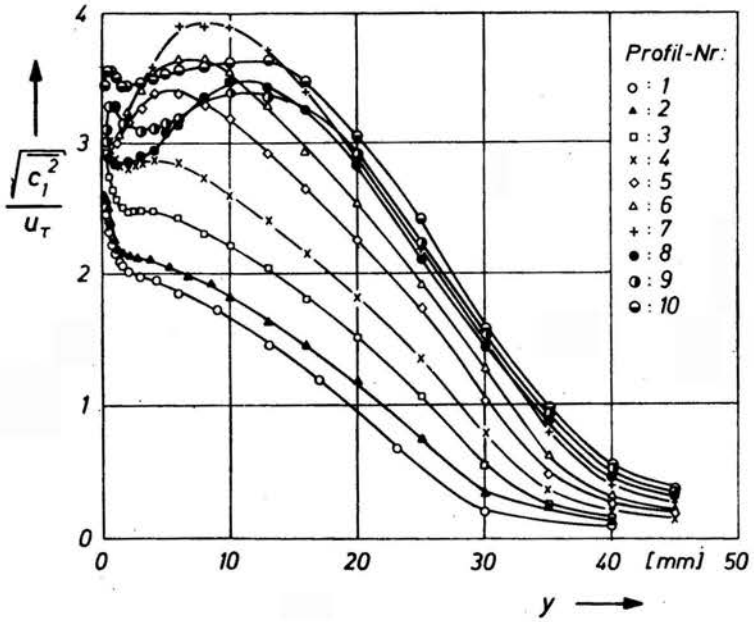

FIG. 10. Turbulence intensity component c_1,

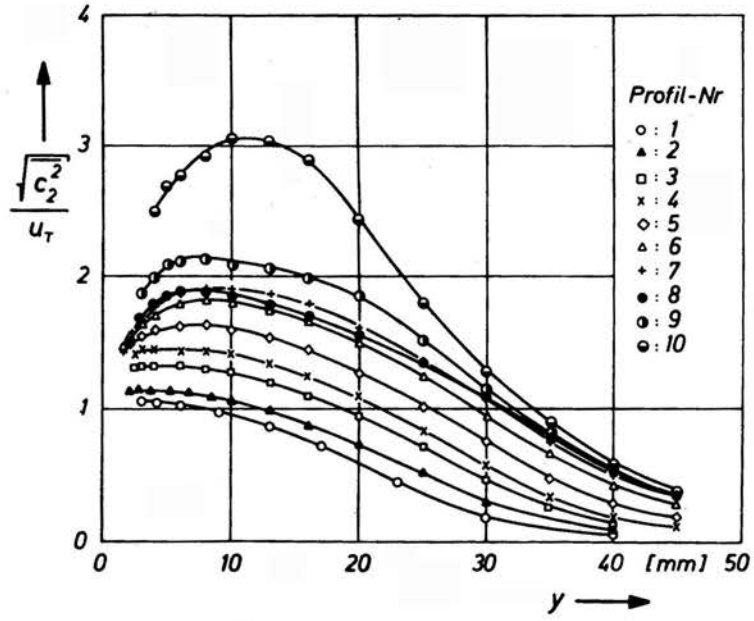

FIG. 11. Turbulence intensity component c_2,

mensional boundary layer because of the extreme conditions existing in this region, as described in Sect. 5.1. At this station the vector of the mean velocity has in the middle part of the boundary layer a component v normal to the wall of about 10% of u_δ; as the

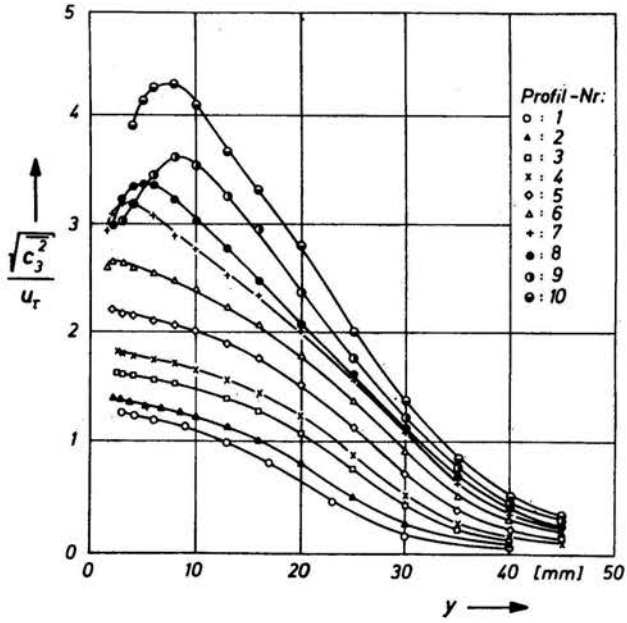

FIG. 12. Turbulence intensity component c_3.

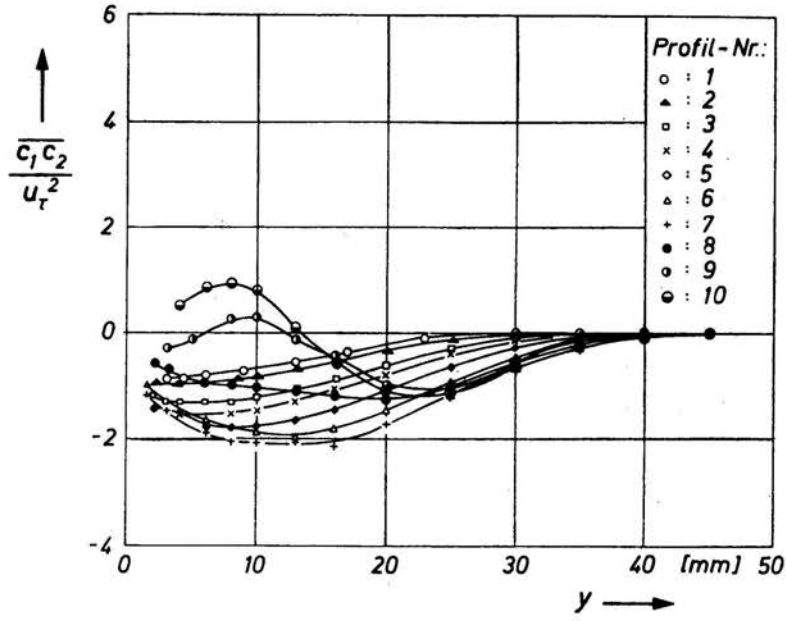

FIG. 13. Shear stress component $\overline{c_1 c_2}$.

wall is approached v first tends to zero and then changes its direction. In addition, the w component grows. This results in the above—mentioned acceleration of the flow near the wall which is produced by a secondary boundary layer originating in the horseshoe

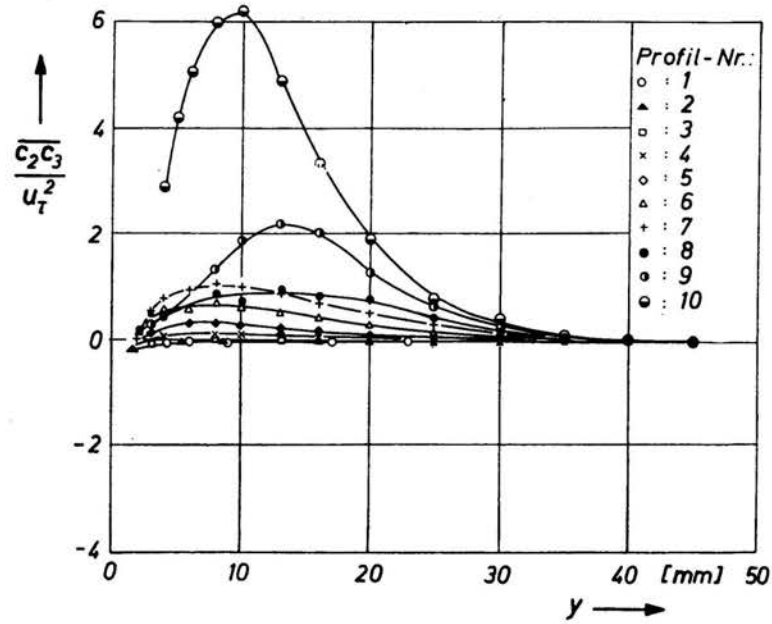

FIG. 14. Shear stress component $\overline{c_2 c_3}$.

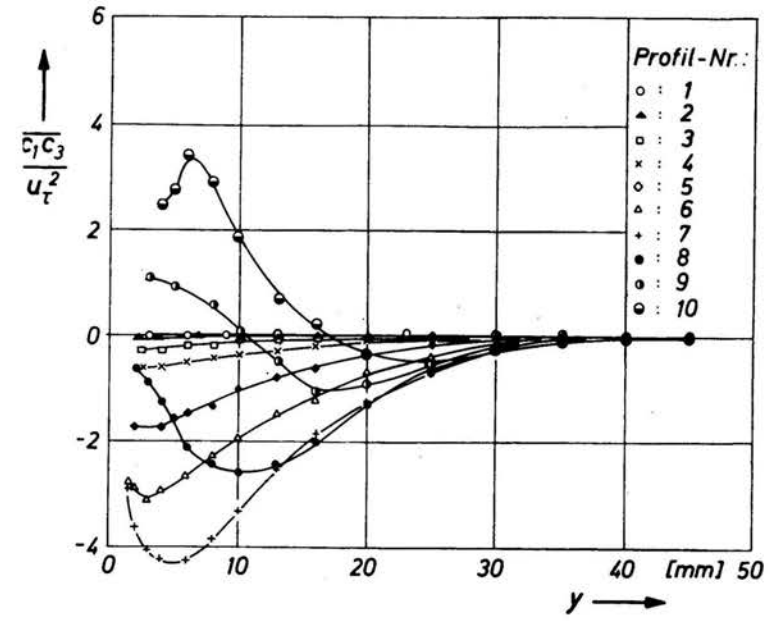

FIG. 15. Shear stress component $\overline{c_1 c_3}$.

vortex at the bottom of the cylinder. A discussion of the behaviour of the stress tensor follows in the next section together with the other related parameters.

As already shown in Fig. 3 the static pressure at the wall and in the free stream differ

in the region near the three-dimensional separation. The profile of the pressure coefficient at Station 10 is shown in Fig. 16. Due to the possibility of errors, these measurements should be interpreted carefully, nevertheless the data do show a large deviation from the assumption of constant pressure inside the boundary layer.

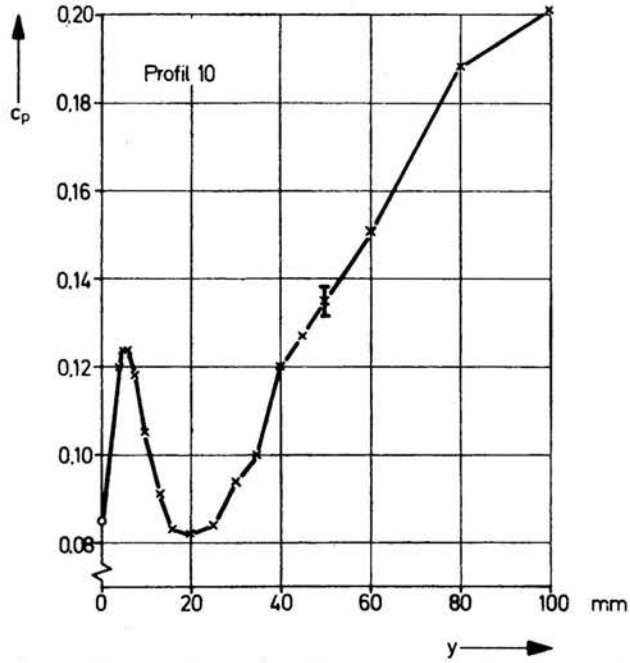

FIG. 16. Pressure coefficient $c_p(y)$, Station 10.

6. Further results

In order to make possible a comparison with existing calculation methods and existing data, other related parameters were computed from the present measurements. It is especially important to include information about the nature of the turbulent shear stresses. In contrast to the two-dimensional case one has to take into account the vectorial nature of the mean velocity and of the shear stress in a three-dimensional boundary layer, i.e. the direction of the different parameters must be considered. Several calculation methods for turbulent boundary layers use empirical equations for the shear stress and relate it to the mean velocity gradient, e.g. the eddy-viscosity or the mixing-length hypothesis. If these equations are to be used in the same way for three-dimensional turbulent boundary layers, the directions of the shear stress and the velocity gradient must be taken into consideration.

If it is assumed that the shear stress component $\overline{c_1 c_3}$ has no influence on the mean velocity profile, the magnitude of the resultant shear stress can be computed by

$$|\tau| = \varrho \cdot \sqrt{\overline{c_1 c_c}^2 + \overline{c_2 c_3}^2},$$

and its angle relative to the x-y-plane of the boundary layer coordinates is given by

$$\gamma_\tau = \operatorname{arctg}\left(\frac{\overline{c_2 c_3}}{\overline{c_1 c_2}}\right) + \gamma \quad \text{for} \quad \overline{c_1 c_2} < 0$$

or

$$\gamma_\tau = \operatorname{arc\,ctg}\left(\frac{\overline{c_1 c_2}}{\overline{c_2 c_3}}\right) + \gamma \quad \text{for} \quad \overline{c_1 c_2} > 0.$$

(N.B. $\overline{c_2 c_3}$ is greater than zero in all measured profiles.)

For computing the magnitude of the velocity gradient vector only the components parallel to the wall are considered:

$$\left|\frac{\partial c}{\partial Y}\right| = \sqrt{\left(\frac{\partial u}{\partial Y}\right)^2 + \left(\frac{\partial w}{\partial Y}\right)^2},$$

and its angle relative to the x-y-plane is thus

$$\gamma_G = \operatorname{arctg}\left(\frac{\partial w}{\partial Y} \Big/ \frac{\partial u}{\partial Y}\right).$$

Other authors have already shown, that the direction of the mean velocity gradient vector and the direction of the result shear stress do not agree in three-dimensional boundary layers (see [2]); this is also the case in the boundary layer investigated here, where very large discrepancies are found.

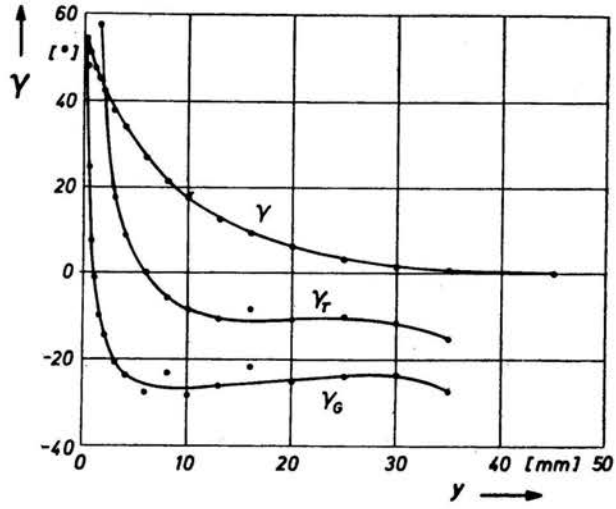

FIG. 17. Direction of mean velocity (γ), velocity gradient (γ_G) and shear stress (γ_τ), station 7.

Figure 17 indicates the magnitude of the discrepancies in the present flow and also contains the yaw angle measured at Station 7.

The eddy-viscosity model relates the shear stress and the velocity gradient via

$$|\tau| = \varrho \nu_e \left|\frac{\partial c}{\partial Y}\right|.$$

Non-dimensionalizing v_e with u_δ and a displacement thickness δ_{1u} (formed from the velocity u), it follows that

$$k_2 = \frac{v_e}{u_\delta \cdot \delta_{1u}},$$

which is often constant for the central part of two-dimensional boundary layer profiles. Figure 18 shows k_2 versus Y/δ (δ = boundary layer thickness) for all stations (without

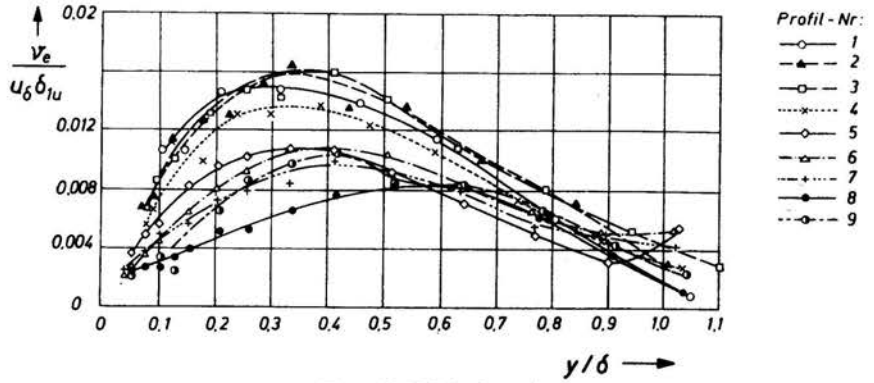

FIG. 18. Eddy viscosity.

Station 10 which is already separated) along the streamline and it may be noted that only at the stations 1, 2 and 3 the shape is similar to the two-dimensional case.

For the mixing length the defining relation is

$$\tau = \varrho l^2 \left| \frac{\partial c}{\partial Y} \right|^2.$$

For 2-D boundary layers we have

$$l = k_1 \cdot Y \quad \text{for} \quad Y/\delta \ll 1, \quad k_1 = 0.41,$$
$$l = c \cdot \delta \quad \text{for} \quad Y/\delta \leqslant 1, \quad c \approx 0.016.$$

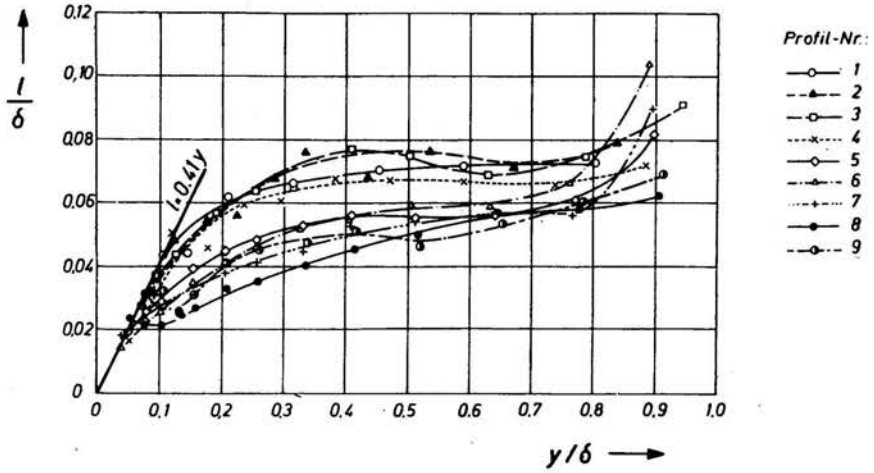

FIG. 19. Mixing length.

Figure 19 shows the mixing length versus the wall distance (both non-dimensionalized with δ) for all stations. Again there exists a large deviation in comparison with the two-dimensional profile at Station 1.

A comparison with the shear stress model of BRADSHAW [8] has shown similar results. Bradshaw stated that the ratio of the Reynolds stress to the turbulence energy is a constant in 2-D boundary layers over about 80% of the boundary layer thickness. Hence for 3-D boundary layers we may infer

$$\frac{|\tau/\varrho|}{q^2} = \frac{\sqrt{\overline{c_1 c_2}^2 + \overline{c_2 c_3}^2}}{\overline{c_1^2} + \overline{c_2^2} + \overline{c_3^2}} = a_1 = \text{const.}$$

Figure 20 shows the result of our measurements. Again only for the first 3 stations the value of a_1 is constant as in the 2-D case.

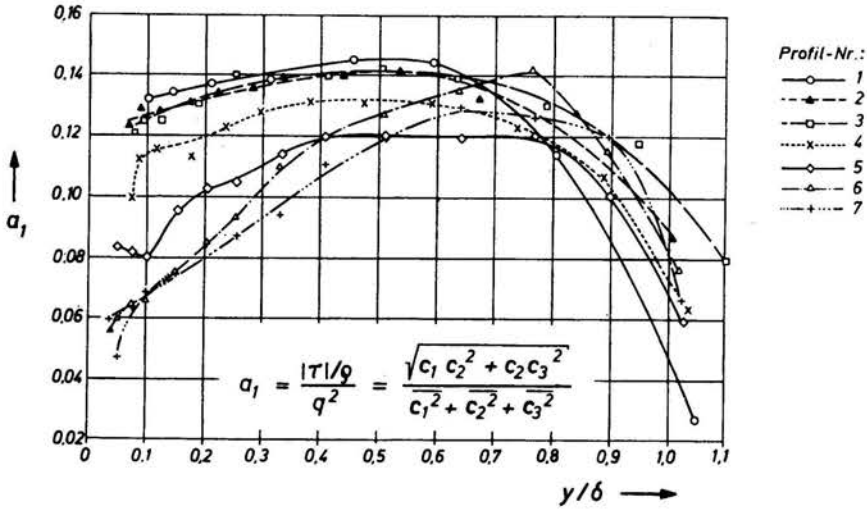

FIG. 20. Ratio of the Reynolds stress to the turbulence energy.

7. Conclusions

The measurements presented in this paper give a comprehensive description of the investigated three-dimensional turbulent boundary layer. Due to the extreme care taken with regard to the measurement techniques, the accuracy and reliability of the present data are believed to be comparatively good. The nature of the turbulent shear stress is the most interesting part of the results, indicating that the shear stress models used in two-dimensional computation methods can not be applied to three-dimensional turbulent boundary layers without additional new empirical input. No correlation could be found between the wall-parallel shear stress and the velocity gradient $\partial c/\partial Y$. In the boundary layer investigated in the present work noticeable gradients exist also in other directions; it therefore seems necessary to examine the relationship between all three components of the shear stress and all components of the velocity gradient vector; to do this, however, further measurements are necessary.

Other results presented here indicate that the applicability of the boundary layer simplifications to three-dimensional turbulent boundary layers (at least those near separation) should be discussed. Further, the results show a good agreement with Elsenaar's data from an infinite swept wing, but the three-dimensional effects are noticeably stronger in the present case.

References

1. B. BERG, A. ELSENAAR, *Measurements in a three-dimensional incompressible turbulent boundary layer in an adverse pressure gradient under infinite swept wing conditions*, NLR TR 72092 U, 1972.
2. A. ELSENAAR, S. H. BOELSMA, *Measurements of the Reynolds stress tensor in a three-dimensional turbulent boundary layer under infinite swept wing conditions*, NLR TR 74095 U, 1975.
3. L. F. EAST, R. P. HOXEY, *Low-speed three-dimensional turbulent boundary layer data, Part I and II*, RAE T.R. 69041 and 69137, 1969.
4. J. O. HINZE, *Turbulence*, 2nd ed., McGraw-Hill 1975.
5. P. BRADSHAW, R. F. JOHNSTON, *Turbulence measurements with hot-wire anemometers*, NPL Notes on Applied Science, 33, 1963.
6. R. DECHOV, *Mittlere Geschwidigkeit und Reynoldsscher Spannungstensor in der dreidimensionalen turbulenten Wandgrenzschicht vor einem stehenden Zylinder*, Dissertation Karlsruhe 1976.
7. P. S. KLEBANOFF, *Characteristics of turbulence in a boundary layer with zero pressure gradient*, NACA Report 1247, 1955.
8. P. BRADSHAW, D. H. FERRISS, N. P. ATWELL, *Calculation of boundary layer development using the turbulent energy equation*, JFM 28, 1967.

INSTITUT FÜR STRÖMUNGLEHRE UND STRÖMUNGSMASCHINEN,
UNIVERSITÄT KARLSRUHE, FRG.

Received October 18, 1977.